

R. M. Trigo · I. F. Trigo · C. C. DaCamara
T. J. Osborn

Climate impact of the European winter blocking episodes from the NCEP/NCAR Reanalyses

Received: 15 July 2003 / Accepted: 9 February 2004 / Published online: 29 May 2004
© Springer-Verlag 2004

Abstract A comprehensive multivariable characterisation of the climatic impacts of winter blocking and strong zonal-flow (non-blocking) episodes over the Euro-Atlantic sector is presented here, using a 40-year (1958–97) consistent dataset from NCEP/NCAR. Anomaly fields of surface or low troposphere climate variables are then interpreted based on large-scale physical mechanisms, namely, the anomalous mean flow (characterised by the 500 hPa geopotential height and the surface wind) and the anomalous eddy activity (characterised by the surface vorticity and cyclonic activity). It is shown that the lower troposphere (850 hPa) temperature patterns are mainly controlled by the advection of heat by the anomalous mean flow. However, at the surface level, the anomaly patterns obtained for maximum and minimum temperatures present important asymmetries, associated with a different control mechanism, namely the modulation of shortwave and longwave radiation by cloud cover variations. It is shown that blocking and non-blocking episodes are typically associated with important meridional shifts in the location of maximum activity of transient eddies. The influence of persistent anomaly events in precipitable water is strongly related to the corresponding anomaly fields of lower troposphere temperature. The precipitation rate, however, appears to be

essentially controlled by the surface vorticity field and preferred locations of associated cyclones.

1 Introduction

The European middle-latitude climate is controlled by the usual sequence of disturbances travelling from the west, with spells of varying precipitation amount alternating with dry periods ranging from the week up to the month scales. However, this pattern is often disrupted by a temporary change to a situation of predominantly meridional flow (Barry and Chorley 1998). Such meridional circulation favours the formation of strong slow-moving or stationary anticyclones at high latitudes (blocking highs), often accompanied by slow-moving or stationary low-pressure areas at lower latitudes (Treidl et al. 1981). Several theories have been proposed for the formation and maintenance of blocking episodes, most of which related to amplification of Rossby waves (Tung and Lindzen 1979), with barotropic (Simmons et al. 1983) or baroclinic (Frederiksen 1982) instability, or as a manifestation of multiple equilibria (Charney and Devore 1979). A significant number of works invoke non-linear interactions, either between zonal flow and eddies (Reinhold and Pierrehumbert 1982), or between planetary waves (Egger 1978; DaCamara et al. 1991; Kung et al. 1990; Christensen and Wiin-Nielsen 1996). A number of authors have pointed to the decisive contribution from high frequency cyclones to develop (e.g. Mullen 1987; Colucci and Alberta, 1996; Nakamura et al. 1997) and sustain (e.g. Shutts 1986) the typical low-frequency anomalies associated with blocking episodes. Conceptual models linking blocking anticyclones and transient eddies have been proposed (Shutts 1983; Tsou and Smith 1990).

Since a single blocked situation can persist for weeks, just a few blocking episodes can determine the climate characteristics of one winter (Stein 2000). In recent

R. M. Trigo (✉) · I. F. Trigo · C. C. DaCamara
Centro de Geofísica da Universidade de Lisboa,
Departamento de Física, Faculdade de Ciências Campo Grande,
Ed C8, Piso 6, 1749-016 Lisbon, Portugal
E-mail: rmtrigo@fc.ul.pt

R. M. Trigo
Departamento de Eng. Civil da Universidade Lusófona, Lisbon,
Portugal

I. F. Trigo · C. C. DaCamara
Instituto de Meteorologia, Lisbon, Portugal

T. J. Osborn
Climatic Research Unit, University of East Anglia, Norwich, UK

years, the analysis of blocking has been extended to general circulation models, both from an operational forecast (e.g. Tibaldi and Molteni 1990; Kung et al. 1990; Tibaldi et al. 1994) or climatological (Anderson 1993; Tibaldi et al. 1997; Sausen et al. 1995; D'Andrea et al. 1998) perspective. This interest arises because the predictability of the European climate is considered to be higher during, and in, areas of blocking (Tibaldi and Molteni 1990). Oddly, there seems to be a lack of studies describing with sufficient detail the influence of these blocking episodes on the Atlantic/European climate. In fact, for the Northern Hemisphere, different authors have either focused their climate impact studies on particular intense blocking episodes over Europe (e.g. Green 1977), the United States (e.g. Quiroz 1984), or have looked at composites from relatively short time series (e.g. Hansen et al. 1993; Quadrelli et al. 2001). Interestingly, the pioneering works by Rex (1950a,b; 1951) are still used as the main reference for this purpose. However, the scope of those studies was limited by the short time series used in all of them. In fact, Rex drew most of his conclusions on blocking influence over European climate based on just two episodes (one in winter and one in summer) in Rex (1950b), increasing to six cases (three in winter and in summer) in his following updated work (Rex 1951, R51 hereafter). It is reasonable to doubt the statistical stability of his results because they are dependent on such a small number of blocking events. The necessity to obtain stable anomaly fields of surface (and upper level) climate variables requires the use of datasets with a much longer period, focusing on a large number of years and including many blocking episodes. Nevertheless, it is only fair to state that Rex makes an impressive use of the (then) recently available 500 hPa charts, as well as several different climate datasets (from a large number of different European Meteorological Offices). To the best of our knowledge, no single study has used long datasets (e.g. 30 years or more) to fully characterize the average climate impact on the lower troposphere using the composite of all blocking episodes (grouped by season of occurrence).

Here, we present an attempt to update and consolidate some of Rex's (1950b; 1951) conclusions for the winter season over the Euro-Atlantic sector based on the extensive use of the NCEP/NCAR Reanalysis dataset with a much longer period (40 years) of consistent data. Moreover, most authors tend to restrict their analysis to the positive anomalies (blocking) episodes neglecting the symmetric, and equally interesting, negative anomalies (strong zonal flow or non-blocking) episodes. In this study the climatic signature of both situations are fully characterized in accordance with the procedure adopted by R51. The main objectives of this study are thus twofold:

a. To present a comprehensive characterization of the climatic impacts of blocking and strong zonal-flow episodes over the Euro-Atlantic sectors using a 40-year period of consistent data. This includes an

analysis of anomaly fields of climate variables rarely employed in previous studies, such as maximum and minimum surface temperatures or precipitable water.

b. To make an explicit use of dynamical variables (e.g. surface anomalous wind and vorticity fields as well as the spatial frequency distributions of individual cyclones) that can provide a physical interpretation of the spatial distribution of climatic anomalies associated with both blocking and non-blocking composites. Some methodological aspects used in this analysis follow closely those adopted in a recent work (Trigo RM et al. 2002, TOC hereafter).

Data and the criteria to define blocking and non-blocking episodes are introduced in Sect. 2. Sects. 3 to 6 illustrate the analysis of the composites for different variables for both blocking and non-blocking composites, namely; 500 hPa geopotential height, 850 hPa temperature, surface maximum and minimum temperatures, precipitable water and precipitation rate. Then the interpretation of the physical mechanisms that generate the anomaly fields of these variables is performed by means of corresponding anomaly fields of surface wind, vorticity and cyclonic activity. Finally a discussion and some conclusions are presented in Sect. 7.

2 Data and blocking definitions

2.1 Data

The data used in this study are large-scale gridded data retrieved from the NCEP/NCAR Reanalysis dataset for the period 1958–1997. The NCEP/NCAR Reanalysis data were derived through a consistent assimilation and modelling procedure that incorporated most available weather and satellite information (Kalnay et al. 1996). While the assimilation system has been frozen throughout the whole re-analysis process, the observation base has undergone significant changes over the considered period (White 2000). Six-hourly values of sea level pressure (SLP), 500 hPa geopotential height, precipitable water (vertical integral of specific humidity), precipitation rate, 850 hPa temperature, daily maximum and minimum 2 m temperatures, and 10 m zonal (u) and meridional (v) wind components were extracted from the NCEP/NCAR 2.5° latitude by 2.5° longitude grid, for the area 80°N–30°N; 60°W–70°E. Daily values are then computed by averaging the six-hourly analyses (with the exception of maximum and minimum temperatures).

Although based on observational data, the Reanalyses are also dependent upon the skill and reliability of the forecast model. Kalnay et al. (1996) categorize the reliance on the model of different types of variables. While variables such as SLP, 500 hPa geopotential height and 850 hPa temperature correspond to observed variables that were analyzed by the model, precipitation rate is a member of the class of variables that are most dependent upon the forecast model. However, it is

necessary to bear in mind that all the analyses performed in this work are based on the use of anomaly composites (mean field removed), thus considerably filtering the impact of systematic biases of the model on our results. However, time dependent biases can still influence results.

2.2 Blocking and non-blocking definition

Since blocking highs affect the middle and upper troposphere as well as the surface they cannot usually be properly identified by inspection of surface synoptic charts alone (Treidl et al. 1981). There is no generally recognized single definition of a blocking event; it is widely accepted, however, that they are related to large geopotential height anomalies at 500 hPa, both in space and time. The criteria used to define blocking episodes have varied from the earlier subjective definitions (e.g. Elliot and Smith 1949; Rex 1950a, 1950b; Austin 1980; Treidl et al. 1981) to more recent objective indices (e.g. Lejenäs and Øakland 1983; Dole 1986; Tibaldi and Molteni 1990; Liu 1994). Here, a similar procedure to that originally developed by Tibaldi and Molteni (1990) is adopted, with the necessary adaptation to the window of data extracted and to the higher resolution of the NCEP/NCAR Reanalysis dataset (2.5° by 2.5° instead of 5° by 5°). Furthermore, we took into consideration the latitudinal frequency distribution of blocking episodes obtained in the comprehensive study of Treidl et al. (1981). Two 500 hPa geopotential height gradients, GHGS and GHGN, are computed for 2.5° longitude intervals over the Euro-Atlantic sector from 27.5°W to 40°E:

$$\begin{aligned} GHGS &= \frac{Z(\lambda, \phi_o) - Z(\lambda, \phi_s)}{\phi_o - \phi_s} \\ GHGN &= \frac{Z(\lambda, \phi_n) - Z(\lambda, \phi_o)}{\phi_n - \phi_o} \end{aligned} \quad (1)$$

$$\begin{aligned} \phi_n &= 77.5^\circ N + \Delta \\ \phi_o &= 60^\circ N + \Delta \\ \phi_s &= 40^\circ N + \Delta \\ \Delta &= -5.0^\circ, -2.5^\circ, 0^\circ, 2.5^\circ \end{aligned}$$

where $Z(\lambda, \phi)$ is 500 hPa height at longitude λ and latitude ϕ . Then, following the procedure developed by Tibaldi and Molteni (1990), a given longitude is defined as “blocked” at a specific instant in time if the following conditions are satisfied for at least one value of Δ :

$$GHGS > 0 \quad \text{and} \quad GHGN < -10 \text{ m/deg lat} . \quad (2)$$

As mentioned previously, most authors tend to restrict their analysis to the positive anomalies (blocking) episodes disregarding the analysis of non-blocking episodes. Here, we define (empirically) an objective index to characterize strong zonal flow episodes. After testing different threshold values we considered that a given longitude is defined as “non-blocked” at a specific

instant in time if the following condition is satisfied for at least one value of Δ :

$$GHGS < -22.5 \text{ m/deg lat} . \quad (3)$$

A certain amount of empirical tuning was applied with the aim of obtaining comparable frequencies of blocked and non-blocked days. Naturally, the use of different thresholds would implicate differences in the total number of “non-blocked” days. The whole Euro-Atlantic (E–A) sector is considered to be blocked (non-blocked) if three or more adjacent longitudes within its limit are blocked (non-blocked). These criteria are considered to be sufficient to define a local (in time and space) blocking pattern (Verdecchia et al. 1996; Tibaldi et al. 1997). To evaluate the seasonal cycle of both types of occurrences, we computed the average frequency of blocked (solid line) and non-blocked (dashed line) days for each month of the year for the E-A sector (Fig. 1a). While the blocking frequency curve presents the well known spring maximum and summer minimum (see, e.g. Fig. 2c in D’Andrea et al. 1998), the corresponding non-blocking frequency curve exhibits an expected winter maximum followed by a pronounced minimum in spring and summer. It is worth noticing that the lack of a minimum duration prerequisite leads to the awkward circumstance whereby the vast majority (~90%) of winter days are considered (individually) to be either blocked or non-blocked. Clearly, a minimum duration threshold must be imposed to the definitions of both blocking and non-blocking patterns.

2.3 The duration of blocking and non-blocking episodes

The typical duration of blocking episodes varies between 5 and 30 days (Treidl et al. 1981; Tibaldi and Molteni 1990). However, similarly to the ambiguity with the blocking definition, there is no minimum duration value for blocking episodes that is globally accepted. In fact, the minimum threshold in literature has varied between three (Elliot and Smith 1949) and ten days (Rex 1950a), while a majority of works tends to adopt a value of five days (Treidl et al. 1981; Dole 1986; Tibaldi and Molteni 1990; D’Andrea et al. 1998). Here, an empirical lower threshold of ten consecutive blocked (or non-blocked) days is added to the circulation constraints defined by the set of Eqs (1) to (3). While this minimum duration value might be considered too restrictive (Sausen et al. 1995) it is, nevertheless, a necessary requirement if one intends to establish a fair comparison of results with those obtained by R51. Following a procedure previously adopted by other authors, we accepted as valid all those blocking (or non-blocking) episodes where a single intermediate day does not fulfill the required conditions (D’Andrea et al. 1998; Verdecchia et al. 1996). For example, if four successive days, considered blocked by the index for a specific sector are followed by one non-blocked day and then by five successive blocked days, the entire episode is considered to be a 10-day blocking

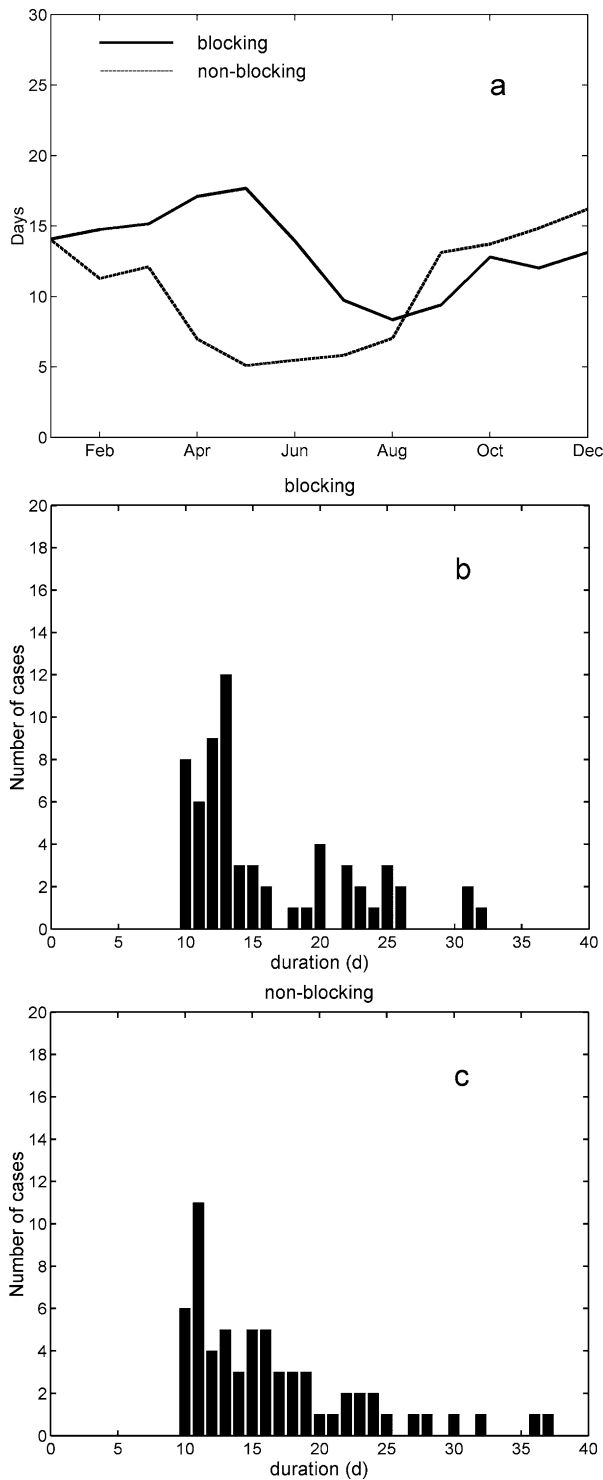


Fig. 1 a Mean frequency of blocked (*solid line*) and non-blocked (*dashed line*) days for each month, for the E-A sector; b Histogram of the duration of blocking episodes with at least 10 days; c the same as b but for non-blocking events

event. A similar tapering criterion procedure was applied to define all non-blocking episodes. Here, the use of wording such as blocking (non-blocking) episode or blocked (non-blocked) day is, from now on, restricted to

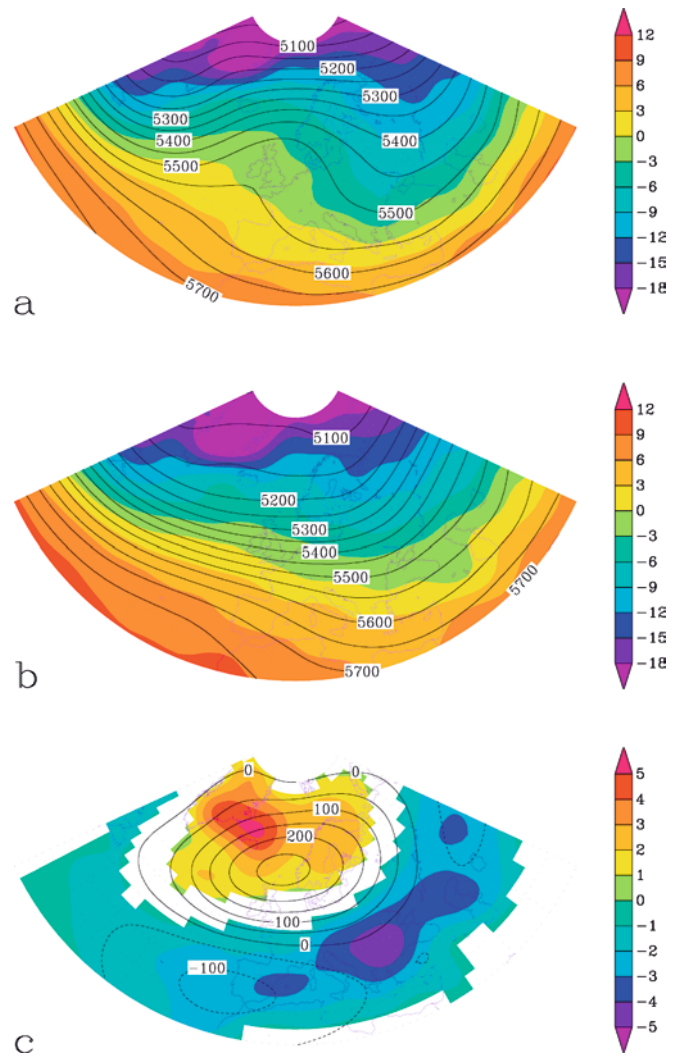


Fig. 2 The mean 500 hPa geopotential height (gpm) anomalies for all winter a blocking, and, b non-blocking episodes, with a minimum duration of 10 days. The shading shows the corresponding 850 hPa temperature field (°C); c Differences between the mean 500 hPa geopotential height (gpm) composites and the corresponding 850 hPa (°C) temperature composites (represented only if significant at the 1% level)

those days and episodes that fulfill the previous filtering criteria.

This procedure was applied to every month of the year but the analysis will be restricted to winter. Accordingly all blocked winter days (DJF) are considered, even if the blocking episode began before December or ended after February. Following recent major works of the climate community that analyze blocking episodes, the DJF winter definition is also used here. Moreover, it is compatible with the work of R51 as his three winter blocking episodes happened either in January or February. Overall, the total number of winter days (3610) taken into consideration by the blocking composite is slightly lower (1051) than those considered by the non-blocking composite (1084). The analysis of the climate impact of blocking and strong zonal flow

(non-blocking) episodes in the next sections will be based on these composites. Finally, the remaining 1475 days (41%) are characterized by intermediate winter circulation conditions.

The total number of blocking and non-blocking episodes considered (lasting at least 10 days) for the winter season, were exactly the same, i.e. 63 cases, and their frequency histogram of duration can be seen in Fig. 1b and c, respectively. Both frequency distributions are skewed, as expected, with median duration values of 13 and 14 days for blocking and non-blocking, respectively. While the duration of non-blocking episodes presents a relatively regular decrease with a long tail, the corresponding duration of blocking cases reveals a less clear picture. In fact, the E–A sector presents a sharp decrease of blocking episodes between 14 and 19 days, increasing to more significant numbers between 20 and 26 days. However, a proper comparison of these frequency histograms with previous results is difficult due to differences in datasets used, but also because most authors tend to compute distribution frequencies on a yearly (not winter) basis (e.g. Treidl et al. 1981; Dole 1986; D’Andrea et al. 1998).

In the following sections composites of several climatic variables are analysed for blocked and non-blocked situations (events lasting at least 10 days only). The respective pairs of blocked and non-blocked composites were tested with a two-tailed *t*-test (null hypothesis of equal means). We should emphasize that the evaluation of the degrees of freedom to estimate the significance of the *t* statistic was based on the restrictive criterion adopted in Hansen et al. (1993), i.e. the *t* statistic was computed taking only into account the number of blocking (63) and non-blocking (63) winter episodes with at least 10 days.

3 Circulation anomalies and associated low-troposphere temperature anomalies

The composites of 500 hPa geopotential height for blocking and non-blocking winter episodes, as defined in the previous section, are shown in Fig. 2. The most important feature corresponds to the intensification of the meridional component of the mid-troposphere circulation that is perfectly visible during blocked situations, up and downstream of the British Isles (Fig. 2a). This configuration is usually associated with the splitting of the jet stream into two distinct branches, a feature that is widely accepted as a trademark of European blocking episodes (Rex 1950a,b; Treidl et al. 1981). On the contrary, non-blocked events are characterized by an intensification of the zonal circulation (Fig. 2b). The corresponding 850 hPa temperature fields for both composites are superimposed in Fig. 2a,b. The differences between blocking and non-blocking composites of 500 hPa geopotential height and 850 hPa temperature are shown in Fig. 2c, with the differences of the 850 hPa composites being represented only if they are significant

at the 1% level. This figure presents two recognizable characteristics of the 500 hPa geopotential height anomaly field: the maximum difference located between Scotland and Scandinavia and the less intense maximum negative difference over Iberia (e.g. Hansen et al. 1993; D’Andrea et al. 1998). The corresponding difference for 850 hPa temperature field presents concentrated positive values between Greenland and Scandinavia with a maximum located to the north of Iceland. On the other hand a significant temperature anomaly sector is spread over a large area between the Azores, in mid-Atlantic, and central Asia, with the lowest values observed over the Balkans. The magnitude and location of these positive and negative low troposphere temperature anomalies is similar to results obtained by Hansen et al. (1993) and Dole (1986), although these authors have employed a considerably shorter period (8 and 11 years, respectively) and lower resolution (5° latitude by 5° longitude) dataset. A comparison of these results with those obtained by R51 is left for Sect. 5 where the blocking impacts on maximum and minimum near-surface temperatures are analyzed in detail.

4 Cyclonic activity

As mentioned in the Introduction, several authors have looked at relationships between cyclones and the development of blocking highs. Several of these studies have either focused on particular intense blocking episodes (e.g. Shutts 1986; Lupo and Smith 1995) or have dealt with conceptual models (e.g. Frederiksen 1982; Shutts 1983; Tsou and Smith 1990). A number of authors have emphasized the decisive contribution from high-frequency cyclones for developing (e.g. Colucci and Alberta 1996; Nakamura et al. 1997) and sustaining (e.g. Shutts 1986; Nakamura and Wallace 1990) most blocking episodes. In particular, the works of Shutts (1983) and Mullen (1987) have considered a mechanism whereby transient eddies act to maintain blocking patterns through the addition of anticyclonic vorticity along their western flank. Lupo and Smith (1995) applied the model developed by Tsou and Smith (1990) and, demonstrated that all the blocking episodes in their study were preceded *in time* by an upstream cyclone. More recently, Michelangeli and Vautard (1998) have confirmed that baroclinic waves are fundamental for the appearance of most blocking episodes. Here, we will make use of the large dataset available in order to analyze spatial patterns of cyclone distribution that occur simultaneously with blocking and non-blocking events. For that purpose cyclones were detected and tracked using a automated procedure (e.g. Murray and Simmonds 1991; Serreze et al. 1997; Trigo IF et al. 1999). Recently, Gulev et al. (2001) have used this technique to compute the winter cyclone activity over the entire Northern Hemisphere using the same NCEP/NCAR dataset as in the present study.

The methodology previously developed for the smaller Mediterranean region (Trigo IF et al. 1999, 2002) has been adapted for the area of the study in the E-A sector. The cyclone detection and tracking algorithm, described in the Appendix, is based on the identification, and consequent tracking of local sea level pressure minima. Previous works have pointed out that the use of SLP instead of the vorticity field tend to produce a poleward displacement of the central low's position and a tendency to favour the detection of the deeper or slower-moving systems (Sinclair 1994; Trigo IF et al. 1999). However, the vorticity field near the surface is considerably noisier than the SLP, leading to the additional problem of selecting the vorticity maxima that correspond to a single cyclone.

The average number of cyclones detected per winter per 5° long \times 5° latitude cell, normalised for 50° N, is plotted in Fig. 3a and b, for blocking and non-blocking composites, respectively. The absolute number of cyclones mapped in Fig. 3 may be slightly underestimated, since fast-moving lows may not be counted in some of the individual grid-boxes due to inadequate temporal resolution of the data (Zolina and Gulev 2002). However, the main purpose of this analysis is to compare the spatial resolution of cyclone counts for blocking and non-blocking situations. As expected, during blocking episodes there is a lack of cyclones travelling over the northeastern Atlantic and through Northern Europe, an area that spans roughly between 45° N and 60° N and between 10° W and 20° E (Fig. 3a). Most cyclones tend to move either along the western margin of the blocking pattern (between Greenland and the Arctic Sea) or through a southeasterly trajectory (between the Iberian Peninsula and the Caspian Sea). This split of the cyclonic activity into two distinct branches has been described in models (e.g. Shutts 1983) and also in a 30-year diagnostic study of baroclinic wave activity by Nakamura and Wallace (1990). On the contrary, strong zonal-flow episodes are characterized by a higher number of cyclone centres crossing the North Atlantic and penetrating Northern Europe. Significant cyclones counts can be seen over the Mediterranean, albeit not as many as in the blocking composite. It is important to keep in mind that this type of cyclone identification algorithm tends to produce some poleward bias (Sinclair 1994) implying that these bands may be located a few degrees north of the actual location of most storm-track trajectories. As expected, the difference in cyclonic activity between these blocking and non-blocking composites presents two significant zonal bands of opposite sign (Fig. 3c).

5 Maximum and minimum surface temperatures

The impact of blocking episodes on the mean temperature of the European region has already been described in previous works (e.g. R51; Dole 1986; Hansen et al. 1993). However, a separate analysis developed inde-

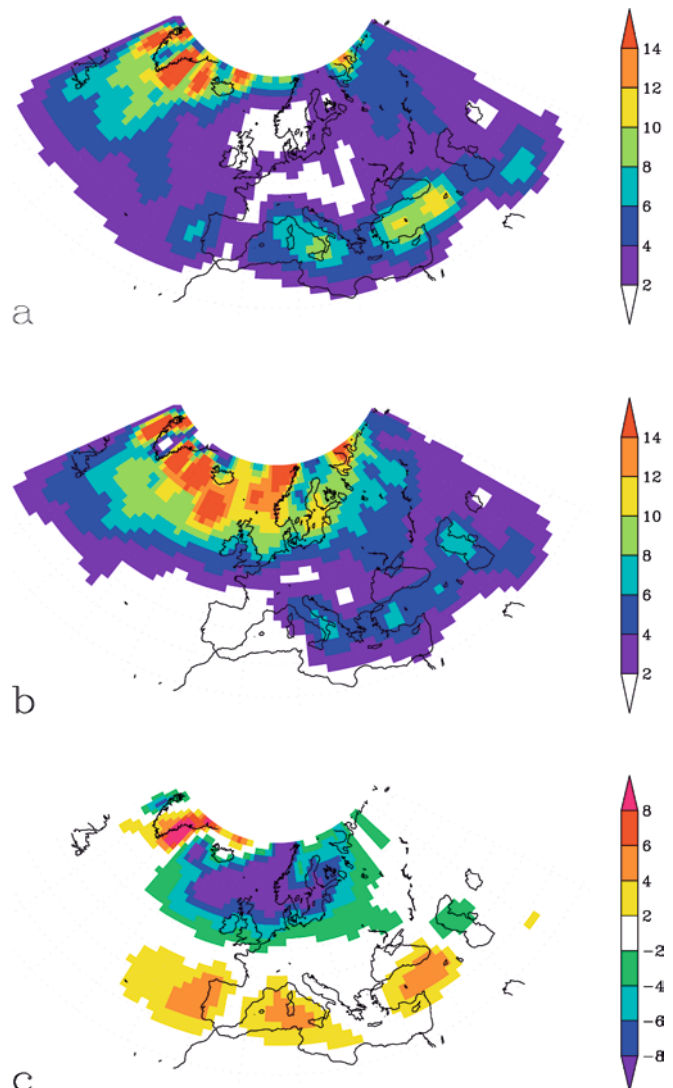


Fig. 3 Number of cyclones per winter, detected per $5^\circ \times 5^\circ$ area normalised for 50° N, for **a** blocking, **b** non-blocking, and **c** their difference

pendently for maximum temperature (T_{\max}), mainly recorded during daytime, and minimum temperature (T_{\min}), usually recorded towards the end of the night, has not previously been attempted. Here, such an analysis is presented, and the anomaly fields of T_{\max} (T_{\min}) for blocking and non-blocking composites can be observed in Fig. 4a,b (Fig. 5a,b). In order to help the interpretation of these fields, the corresponding anomalous mean atmospheric flow is also shown in both figures through the 10 m wind velocity anomalies. All anomaly fields were computed by removing the respective winter climatology from the composite fields. Near surface NCEP/NCAR winds present some problems, including time-dependent biases, over the North Atlantic ocean area (Cox et al. 2000). Nevertheless, their validation against independent observed data is very difficult and the use of composite analysis should considerably diminish the problem.

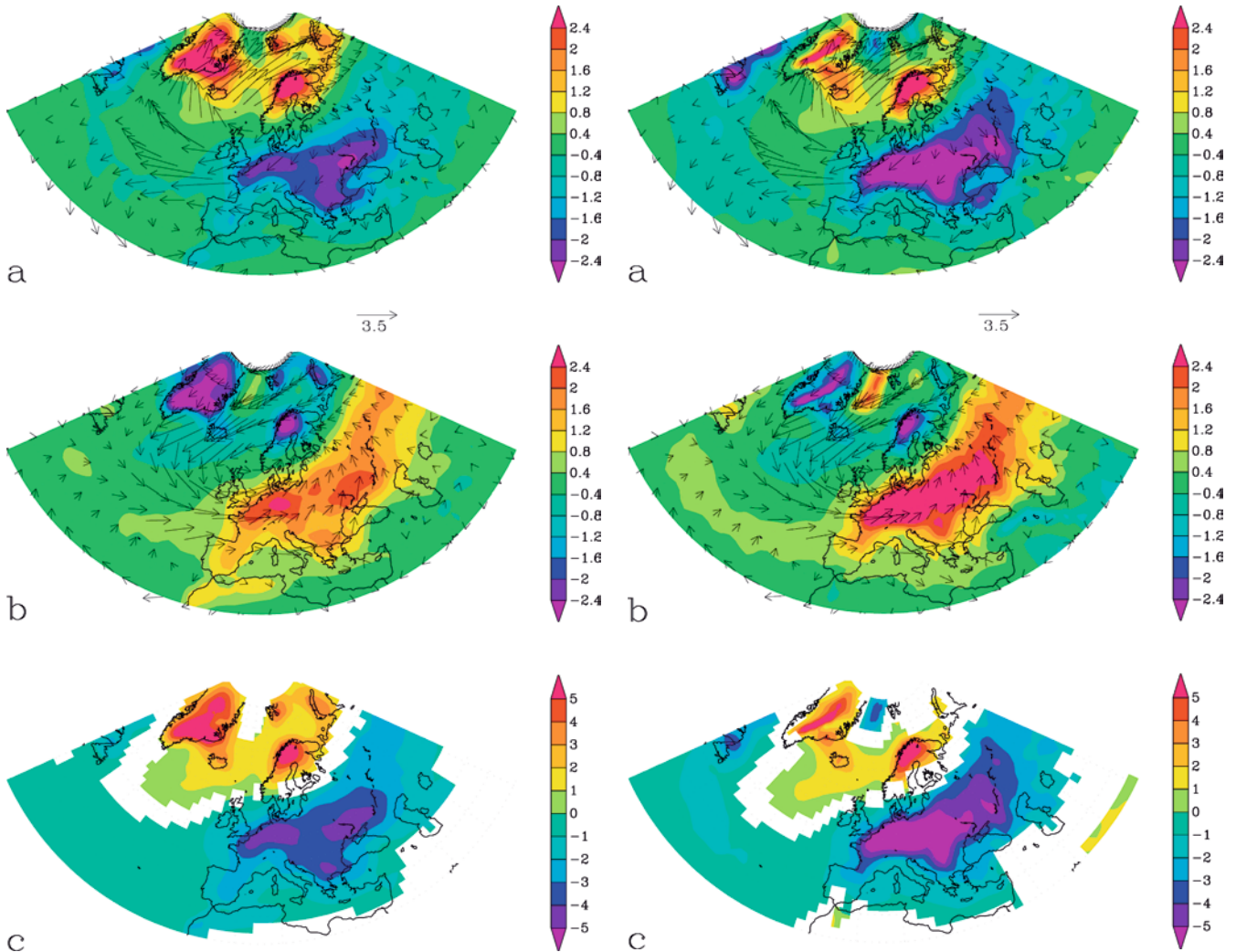


Fig. 4 Anomalies of the daily maximum temperature field ($^{\circ}\text{C}$) for winter composites of **a** blocking episodes, **b** non-blocking episodes, and **c** their difference (represented only if significant at the 1% level). The *arrows* show the respective anomaly of the 10 m wind field (ms^{-1})

During blocking episodes, the meridional SLP gradient is weakened, favouring an advection of cold air from northern Russia into the whole European continent; such cold advection is reflected in the large area of negative anomalies of both Tmax (Fig. 4a) and Tmin (Fig. 5a). However, the magnitude of the temperature anomaly fields over Europe and the extent over Northern Africa is clearly distinct between Tmax and Tmin. The magnitude of Tmin anomalies in Central Europe is considerably stronger than that of Tmax. The reverse can be observed over the Greenland region where the Tmax signal is stronger than that of Tmin. In a previous work (TOC) it was shown that the North Atlantic Oscillation produced the appearance of similar asymmetric patterns that can generate different day and night-time temperature anomalies. The asymmetric responses of the

Fig. 5a–c As in Fig. 4 but for the daily minimum temperature field

Tmax and Tmin fields over northern and eastern continental Europe are mainly caused by the usual lack of clouds that characterises typical blocking anticyclones (Wilby et al. 1997), and thus by the additional night-time outgoing longwave radiation, associated with mostly cloud-free areas. The spatial extent of anomalies, of the order of -0.4 to -1.6 K for blocking composites, covers much of the Iberian Peninsula, Morocco and Algeria even extending to the south of the Caspian Sea for (daytime) Tmax (Fig. 4a), but not for the (night-time) Tmin (Fig. 5a). As shown in Sect. 4, the Mediterranean region is affected by higher than usual storm activity, likely to be associated with increased cloud cover during blocking winter events. Thus, the likely presence of a thick cloud cover does not allow the daytime radiative warming by short-wave solar radiation, while during the night it enhances the greenhouse effect partially offsetting the advection of cold polar air to yield small Tmin anomalies. The small positive temperature anomaly over parts of Greenland, northern Scandinavia and the northern Atlantic in blocking composites results from

enhanced northward advection of warm low troposphere air from the Atlantic.

During strong zonal flow (non-blocking) episodes, the meridional SLP gradient is enhanced, contributing to the strengthening of the westerly wind field (Figs. 4b and 5b). Such strengthening of the westerlies is responsible for an increased advection of moist warm air into Europe, in accordance with the presence of enhanced storm tracks (Fig. 3b), and generates a strong positive temperature anomaly between France and western Russia. Similarly to the blocking composites, the spatial extent of the anomaly fields is larger for T_{\max} than for T_{\min} , while the magnitude of both the negative and positive anomaly patterns is higher for T_{\min} than for T_{\max} over central Europe (Figs. 4a and 5b). As for the blocked case, the difference in day and night-time temperature response during strong zonal flow episodes can be understood by the influence on radiative fluxes of anomalous cloud cover to the south of the storm track anomalies (Figs. 3b,c). A weak cold anomaly develops in both T_{\min} and T_{\max} over Greenland and northern Scandinavia as a consequence of the cold polar air advection from the arctic (Figs. 4b, 5b).

Significant differences at the 1% level in T_{\max} (T_{\min}), between composites of blocked and non-blocked periods, can be seen in Fig. 4c (Fig. 5c). As expected, significant positive differences of both T_{\max} and T_{\min} fields are confined to the northern Atlantic, extending from Greenland to northern Scandinavia, and are slightly larger for T_{\max} than for T_{\min} . However, over the northern sea, both these fields present anomalies that are slightly weaker than the equivalent temperature anomalies at the 850 hPa level. The amplitude of the differences over Europe is higher for T_{\min} than for T_{\max} , but the spatial extent of significant differences over the northern Africa and Caspian Sea sectors is larger for T_{\max} than for T_{\min} .

6 Precipitation

In Sects. 3 and 4 we showed that changes of the mean circulation are accompanied by important shifts of the associated frequencies of cyclones. In this section it will be shown how such shifts can be directly linked with significant changes of regional precipitation over most of Europe and parts of northern Africa. Here, two precipitation-related variables from the NCEP/NCAR Reanalyses, namely, daily precipitation rate and precipitable water (hereafter PR and PW, respectively) are used. It is worth keeping in mind that although the Reanalyses are based on observational data, they are strongly dependent upon the skill and reliability of the model. Kalnay et al. (1996) categorize the reliance on the model of different types of variable; PR is a member of the class of variables that are most dependent upon the forecast model, and model systematic errors may introduce erroneous precipitation data. Nevertheless, NCEP/NCAR Reanalysis precipitation has been shown

to present some skill in comparison with observations (e.g. Widmann and Bretherton 2000). The ability of the NCEP/NCAR reanalysis to reproduce the daily precipitation over Europe was further analyzed by Reid et al. (2001). These authors have shown that, at least, for both England and Italy the reanalysis presents a seasonal cycle in skill, being higher in the winter and lower in the summer. White (2000) shows a discrepancy between NCEP/NCAR global precipitation trend and that observed with the well known climatology by Xie and Arkin (1997). The decline in the number of observations reported by shipping could be partially responsible for such change. Furthermore, the use of composite anomalies eliminates the impact of model inadequacies, in particular those associated with a poor simulation of the precipitation rate mean field (TOC). Finally, it should be stressed that PR is dynamically consistent with other variables used in this study.

PR anomaly fields for composites of winter days characteristic of blocking and non-blocking episodes are shown in Fig. 6a and b, respectively. The most prominent feature in Fig. 6a (Fig. 6b) is the existence of three latitudinal bands of opposite anomaly signs with the largest regions of dry (wet) anomaly values centred roughly near the British Isles and wet (dry) west of the Iberian Peninsula for blocked (non-blocked) composites. Figure 6c shows three latitudinal bands of opposite anomaly signs, where differences between blocking and non-blocking episodes are significant at the 5% level. Significant negative differences of PR are concentrated between Iceland and the Volga river region with minima located west of Scotland, southern Norway and northern France. A prominent positive anomaly appears in eastern Greenland as a result of advection of warm and moist air to the mountainous eastern coast of Greenland. At lower latitudes, a significant positive band of PR extends from the Azores Islands (mid-Atlantic) to southern Iberia with a weaker, but still significant elongation into the Mediterranean basin. In a previous work (Trigo and DaCamara 2000) results from an objective weather type classification showed that the winter precipitation regime in southern Portugal was mainly controlled by days of cyclonic type. In the present context this feature might be associated to the effect of cut-off lows travelling along the southern flanks of blocking highs located in Northern Europe. Finally, a smaller and less consistent positive anomaly can be observed between Greenland and northern Russia.

As previously shown in TOC, enhanced precipitation can be explained by a combination of enhanced moisture availability and/or conditions that enhance condensation of water vapour. It is widely recognized that precipitable water (PW) provides a measure of the first term, being the total water vapour content in a vertical column of the atmosphere. PW anomaly fields for blocking and non-blocking composites of winter days are shown in Figs. 7a,b, respectively. The impact of both blocked and non-blocked circulation is characterised by two bands of positive and negative regions of

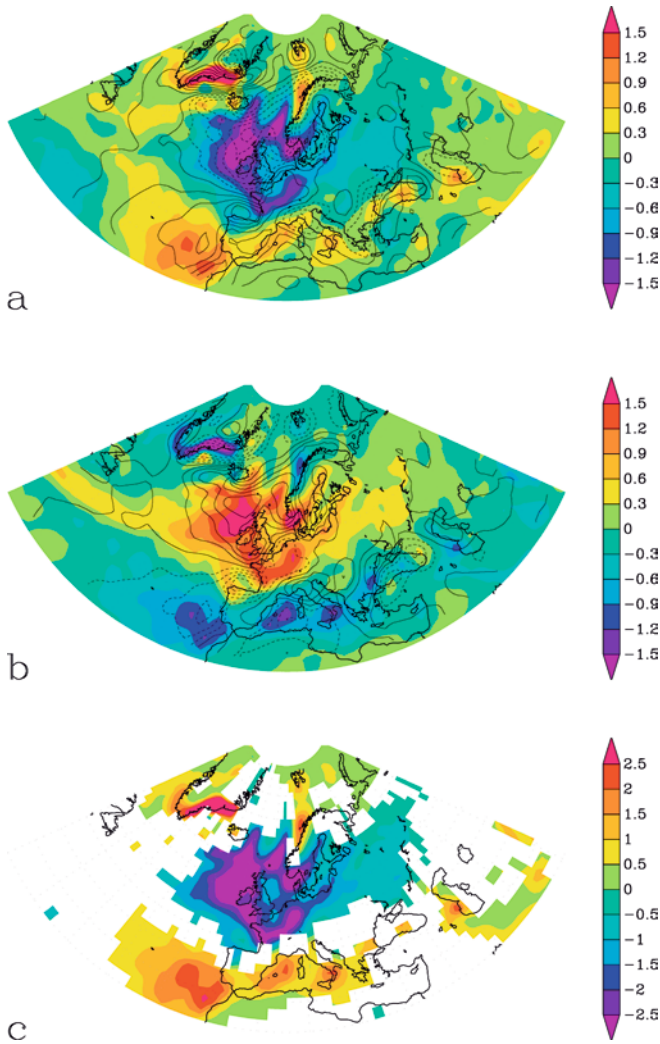


Fig. 6 Anomalies of the precipitation rate (mm/day) for winter composites of **a** blocking episodes, **b** non-blocking episodes, and **c** their difference (represented only if significant at the 5% level). Positive (solid) and negative (dashed) isolines of the 10 m vorticity anomaly field, with intervals in $0.2 \times 10^{-6} \text{ s}^{-1}$, for **a** blocking, and **b** non-blocking composites are also represented)

PW with a slight SW-NE slope. In fact, Fig. 7a (Fig. 7b) shows that the blocking (non-blocking) composite presents a positive (negative) anomaly band extending, with a southwestern-northeastern orientation, from southern Azores region across Central Europe and into the Black Sea region. This diagonal band is bordered by a northern band of opposite sign, extending from the southern Greenland Sea into northern Scandinavia and with a maximum value over Iceland. The spatial extent of these two regions is confirmed in Fig. 7c where all significant differences of PW at the 1% level, between composites of blocked and non-blocked can be seen. It is well known that the water vapor content of the atmosphere is highly associated with its temperature, explaining the similarity of Figs. 7c and 2c (the main difference being the latitude of the southwestern anomaly).

Condensation of the PW content typically requires uplift provided by a range of mechanisms (e.g. Barry

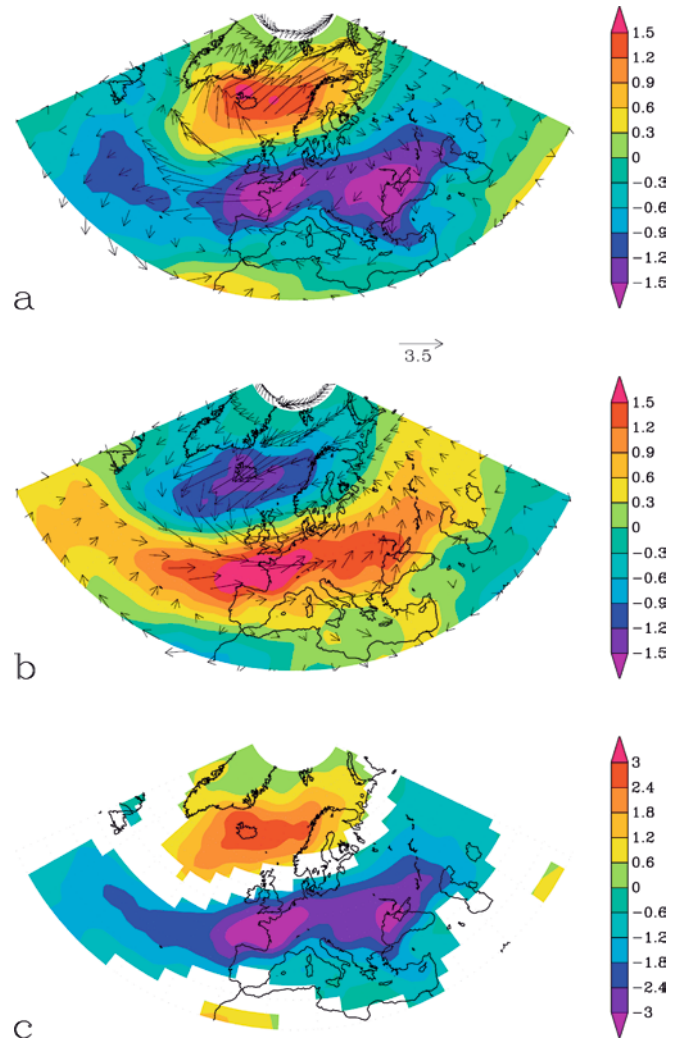


Fig. 7a–c As in Fig. 4 but for precipitable water

and Chorley 1998), but mainly through low-level convergence associated with cyclonic circulation (i.e. positive vorticity). In fact, the relative vorticity field, computed from the composites of both components (zonal and meridional) of the 10 m wind field, indicates that much of the PR response to blocked (Fig. 6a) and strong zonal-flow (Fig. 6b) is associated with anomalous values of the vorticity field. The maximum value of positive (negative) vorticity, represented by solid (dashed) lines is consistently located over (or a few degrees north of) regions with higher (lower) than average PR values. Small northward shifts of the vorticity extreme are compatible with the typical configuration of a mid-latitude synoptic disturbance, with low-pressure centres positioned poleward of the fronts that induce precipitation through strong vertical motions. Furthermore, these extremes of the vorticity field are, generally, in agreement with the location of extreme values of cyclones detected (Fig. 3c). In some locations, the clear relationship between the precipitation and vorticity anomalies is modified by variations in the moisture content of the atmosphere (Fig. 7). For example, the

positive vorticity anomaly over the Bay of Biscay during the blocked composite (Fig. 6a) is not associated with enhanced precipitation, because the moisture content is strongly reduced there (Fig. 7a).

In summary, PR anomalies (Fig. 6, colours) can be mainly attributed to the vorticity of the mean composite circulation (Fig. 6, isolines), that are associated with preferred location of storms as previously described (Fig. 3) and, to a lesser extent, with variations in moisture content (Fig. 7).

7 Discussion and conclusions

Here, we presented a comprehensive characterization of the climatic impacts of blocking and strong zonal-flow episodes over a large area (that encompasses the E-A sector) using the 40-year period of NCEP/NCAR Reanalyses data. Moreover, and unlike many previous authors, we focused our effort equally on the impacts of the positive anomalies (blocking episodes) and on the impacts of the negative anomalies (strong zonal flow or non-blocking episodes). Overall, it is possible to state that there are significant impacts of blocking and non-blocking episodes on all surface or low-troposphere climate variables considered as well as on the associated variables that characterize the tropospheric dynamics. In fact, the use of a stringent t -test to compare differences between composites allowed for a correct assessment of the spatial extent of all significant differences.

The pattern of 850 hPa temperature anomaly can be clearly explained in terms of anomalous mean flow as represented by the 500 hPa height anomaly field. This simple balance is then perturbed by the heat transport associated with transient eddies. The composite analysis of the cyclonic activity for both blocked and non-blocked composites shows a strong meridional shift over Europe, which is directly associated with an equivalent meridional shift in the precipitation pattern. Daily maximum (Tmax) and minimum (Tmin) temperatures present anomaly patterns broadly similar to those of the 850 hPa temperature anomaly field. However, over the northern sea, both Tmax and Tmin anomalies are weaker than the equivalent temperature anomalies depicted at the 850 hPa level. Furthermore, there are obvious asymmetries between the magnitude and spatial extent of Tmax and Tmin anomaly patterns over Europe, northern Africa and around the Caspian Sea region. In a previous work, a similar analysis of the impact of the North Atlantic Oscillation over Europe (Trigo RM et al. 2002) resulted in even larger asymmetries between Tmin and Tmax patterns which were shown to be linked with the corresponding cloud cover patterns. Here, we invoke the same additional mechanism, namely the modulation of shortwave and longwave radiation by cloud cover variations associated with the blocking episodes, to explain these differences between daily Tmax and Tmin anomaly patterns.

In summary, the large-scale mean temperature anomalies can be mostly explained by advective heat transport by the corresponding anomalous mean atmospheric flow (as represented by the 10 m wind velocity anomalies superposed on Figs. 4 and 5). This result is in agreement with Mullen (1987) who showed that the thermal anomalies of the blocking pattern are maintained mainly by the advection of mean temperature by the mean anomalous wind ($-\bar{V} \cdot \nabla \bar{T}$). The cyclones (transient eddies) identified in Sect. 4 tend to partially off-set the zonal asymmetry of the thermal field (Mullen 1987). However, the present analysis highlights the importance of a third process, namely the modulation by anomalous cloud cover (associated with anomalous atmospheric circulation) of the radiative transfer of heat to and from the Earth's surface. These radiative and cloud cover influences, under blocking and strong zonal flow regimes, result in the generation of different day and night-time temperature anomalies.

A full comparison of these results with those obtained by R51 should be done carefully, taking into consideration differences in datasets and methodology applied in both studies, namely:

1. R51 considered the aggregated impact of 3 blocking events while we take 63 into consideration.
2. R51 focused his attention on the mean surface temperature while we study separately the impact on the minimum and maximum temperatures.
3. Finally, R51 employed observed values that were physically measured in a non-regular grid (synoptic stations) while we used “assimilated” values computed by the Reanalyses procedure over a regular grid.

Overall, the location of the positive and negative anomalies obtained in the present study are fairly coincident with those obtained by R51: though the negative temperature anomaly obtained by Rex (1951) does not present an eastern elongation into Russia (see Fig. 5 in R51). Furthermore, the small number of cases taken into consideration in R51 leads to maximum (minimum) extreme values to be several degrees higher (lower) than those obtained here.

For precipitation-related variables, we find distinct patterns of precipitable water (PW) content and precipitation rate (PR) associated with blocking and non-blocking composites. While the former is strongly controlled by the corresponding anomaly fields of the lower troposphere temperature, PR (as estimated by the NCEP/NCAR Reanalysis system) appears to be essentially related to atmospheric circulation patterns that lead to the condensation of the available moisture. These circulation patterns are examined here through the vorticity of the composite of the 10 m wind field and by the actual computation of the spatial frequency of storms.

It is interesting to compare these results with the corresponding precipitation anomaly pattern obtained

by R51. Similar to temperature, and despite the small number of blocking episodes considered by R51, the general location of negative and positive anomaly sectors is similar to those obtained here (compare Fig. 6a with Fig. 7 of R51). These include the important wetter than normal anomalies over southern Iberia, northern Morocco, east Greenland and northern Norway. However, R51 results are somewhat drier than those presented here for most Eastern Europe, including Turkey, the Balkans and also north of the Arctic polar circle.

The two main objectives of this study consisted of: (1) updating some of Rex's (1950b, 1951) conclusions, using climate variable rarely employed in previous studies, such as maximum and minimum surface temperatures or precipitable water; and (2) making use of dynamical variables (e.g. surface anomalous wind and vorticity fields as well as individual cyclones) to provide a physical interpretation. Further work is underway to extend the present analysis to the remaining seasons, including the summer (to compare with Rex 1951 results) and also spring where blocking frequency reaches a yearly maximum in the E-A sector.

Acknowledgements The Reanalyses data have been produced by the NCEP and NCAR DSS. The window (30°N–80°N, 60°E–70°W) has been extracted and kindly provided by Ian Harris and David Viner (CRU). The authors would like to acknowledge Dr. Jean Palutikof and Ms. Célia Gouveia for their helpful suggestions.

8 Appendix

8.1 Cyclone tracking algorithm

The detection and tracking of North Atlantic cyclones is based on an algorithm previously developed for the Mediterranean region by Trigo IF et al. (1999). Both the detection and tracking schemes are performed using 6-hourly sea level pressure (SLP), available from NCEP/NCAR reanalyses on a $2.5^\circ \times 2.5^\circ$ grid. The data cover the area from 30°N to 80°N and 60°W to 70°E, and the period 1958–97.

A candidate cyclone is identified as a local SLP minimum, over a 3×3 grid point area. To be considered a cyclone, this minimum must fulfil two thresholds found empirically:

1. A maximum value of 1020 hPa is required for the central sea level pressure
2. The mean pressure gradient, estimated for an area of 12.5° long. \times 10° lat. around the minimum pressure, must be at least 0.55 hPa/100 km

The cyclone tracking algorithm is based on a nearest-neighbour search procedure (as in Blender et al. 1997; Serreze et al. 1997): a cyclone's trajectory is determined by computing the distance to cyclones detected in the previous chart and assuming the cyclone has taken the path of minimum distance; if the nearest neighbor in

the previous chart is not within an area determined by imposing a maximum cyclone velocity of 50 km/h in the westward direction and of 110 km/h in any other, then cyclogenesis is assumed to have occurred. Again, these thresholds were determined empirically by observing cyclone behaviour in SLP charts.

References

- Anderson JL (1993) The climatology of blocking in a numerical forecast model. *J Clim* 6: 1041–1056
- Austin JF (1980) The blocking of middle latitude westerly winds by planetary waves. *Q J R Meteorol Soc* 106: 327–350
- Barry RG, Chorley RJ (1998) *Atmosphere, weather and climate*. Routledge, London, pp 409
- Blender RK (1997) Identification of cyclone track regimes in the North Atlantic. *Q J R Meteorol Soc* 123: 727–741
- Charney JG, Devore JG (1979) Multiple flow equilibria in the atmosphere and blocking. *J Atmos Sci* 36: 1205–1216
- Christensen WC, Wiin-Nielsen A (1996) Blocking as a wave-wave interaction. *Tellus* 48A: 254–271
- Colucci SJ, Alberta TL (1996) Planetary-scale climatology of explosive cyclogenesis and blocking. *Mon Weather Rev* 124: 2509–2520
- Cox AT, Cardone V, Swail VR (2000) Proc 2nd Int Conf on Reanalyse, Reading, United Kingdom. World Meteorological Organization, Geneva Switzerland. WCRP-109 (WMO/TD876), 73–76
- D'Andrea F, Tibaldi S, Blackburn M, Boer G, Déqué M, Dix RM, Dugas B, Ferranti L, Iwasaki T, Kitoh A, Pope V, Randall D, Roeckner E, Strauss D, Stern W, van Den Dool H, Williamson D (1998) Northern Hemisphere atmospheric blocking as simulated by 15 atmospheric general circulation models in the period 1979–1988. *Clim Dyn* 14: 385–407
- DaCamara CC, Kung EC, Baker WE, Lee BC, Corte-Real JAM (1991) Long-term analysis of planetary wave activities and blocking circulation in the Northern Hemisphere winter. *Beitr Phys Atmos* 64: 285–298
- Dole RM (1986) Persistent anomalies of the extratropical Northern Hemisphere wintertime circulation: structure. *Mon Weather Rev* 114: 178–207
- Egger J (1978) Dynamics of blocking highs. *J Atmos Sci* 35: 1788–1801
- Elliot RD, Smith TB (1949) A study of the effect of large blocking highs on the general circulation in the northern hemisphere westerlies. *J Meteorol* 6: 67–85
- Frederiksen JS (1982) A unified three-dimensional instability theory of the onset of blocking and cyclogenesis. *J Atmos Sci* 39: 969–987
- Green JSA (1977) The weather during July 1976: some dynamical considerations of the drought. *Weather* 32: 120–126
- Gulev SK, Zolina O, Grigoriev S (2001) Extratropical cyclone variability in the Northern Hemisphere winter from the NCEP/NCAR reanalysis data. *Clim Dyn* 17: 795–809
- Hansen AR, Pandolfo JP, Sutera A (1993) Midtropospheric flow regimes and persistent wintertime anomalies of surface-layer pressure and temperature. *J Clim* 6: 2136–2143
- Kalnay E, Kanamitsu M, Kistler R, Collins W, Deaven D, Gandin L, Iredell M, Saha S, White G, Wollen J, Zhu Y, Leetmaa A, Reynolds R, Chelliah M, Ebisuzaki W, Higgins W, Janowiak J, Mo KC, Ropelewski C, Wang J, Jenne R, Joseph D (1996) The NCEP/NCAR 40-years reanalyses project. *Bull Am Meteorol Soc* 77: 437–471
- Kung EC, DaCamara CC, Baker WE, Susskind J, Park CK (1990) Simulations of winter blocking episodes using observed sea surface temperatures. *Q J R Meteorol Soc* 116: 1053–1070
- Lejenäs H, Øakland H (1983) Characteristics of northern hemisphere blocking as determined from long time series of observational data. *Tellus* 35A: 350–362

- Liu Q (1994) On the definition and persistence of blocking. *Tellus* 46A: 286–290
- Lupo AR, Smith PJ (1994) Climatological features of blocking anticyclones in the Northern Hemisphere. *Tellus* 47A: 439–456
- Michelangeli PA, Vautard R (1998) The dynamics of Euro-Atlantic blocking onsets. *Q J R Meteorol Soc* 124: 1045–1070
- Mullen SL (1987) Transient eddy forcing of blocking flows. *J Atmos Sci* 44: 3–22
- Murray RJ, Simmonds I (1991) A numerical scheme for tracking cyclones centres from digital data. Part I. Development and operation of the scheme. *Aust Meteorol Mag* 39: 155–166
- Nakamura H, Wallace JM (1990) Observed changes in baroclinic wave activity during the life cycles of low-frequency circulation anomalies. *J Atmos Sci* 47: 1100–1116
- Nakamura H, Nakamura M, Anderson JL (1997) The role of high- and low-frequency dynamics in blocking formation. *Mon Weather Rev* 125: 2074–2093
- Quadrelli R, Pavan V, Molteni F (2001) Wintertime variability of Mediterranean precipitation and its links with large-scale circulation anomalies. *Clim Dyn* 17: 457–466
- Quiroz RS (1984) The climate of 1983–84 winter. A season of strong blocking and severe cold in North America. *Mon Weather Rev* 112: 1894–1912
- Reid PA, Jones PD, Brown O, Goodess CM, Davies TD (2001) Assessments of the reliability of NCEP circulation data and relationships with surface climate by direct comparisons with station based data. *Clim Res* 17: 247–261
- Reinhold BB, Pierrehumbert RT (1982) Dynamics of weather regimes: quasi-stationary waves and blocking. *Mon Weather Rev* 110:1105–1145
- Rex DF (1950a) Blocking action in the middle troposphere and its effect upon regional climate. Part I. An aerological study of blocking action. *Tellus* 2: 196–211
- Rex DF (1950b) Blocking action in the middle troposphere and its effect upon regional climate. Part II. The climatology of blocking action. *Tellus* 2: 275–301
- Rex DF (1951) The effect of Atlantic blocking action upon European climate. *Tellus* 3: 1–16
- Sausen R, König W, Sielmann F (1995) Analysis of blocking events observation and ECHAM model simulations. *Tellus* 47A: 421–438
- Serreze MC, Carse F, Barry RG, Rogers JC (1997) Icelandic Low cyclone activity: climatological features, linkages with the NAO, and relationships with recent changes in the Northern Hemisphere circulation. *J Clim* 10: 453–464
- Shutts GJ (1983) The propagation of eddies in diffluent jet streams: eddy forcing of “blocking” flow fields. *Q J R Meteorol Soc* 109: 737–762
- Shutts GJ (1986) A case study of eddy forcing during an Atlantic blocking episode. In: Benzi R, Saltzman B, Wiin-Nielsen AC (eds) *Anomalous atmospheric flows and blocking*. *Advances in Geophysics*, vol 29, Academic Press, New-York, pp 135–162
- Sinclair MR (1994) An objective cyclone climatology for Southern Hemisphere. *Mon Weather Rev* 122: 1156–1167
- Simmons AJ, Wallace JM, Branstator GW (1983) Barotropic wave propagation and instability, and atmospheric teleconnection patterns. *J Atmos Sci* 40: 1363–91
- Stein O (2000) The variability of Atlantic-European blocking as derived from long SLP time series. *Tellus* 52A: 225–236
- Tibaldi S, Molteni F (1990) On the operational predictability of blocking. *Tellus* 42A: 343–365
- Tibaldi S, Tosi E, Navarra A, Pedulli L (1994) Northern and Southern Hemisphere seasonal variability of blocking frequency and predictability. *Mon Weather Rev* 122: 1971–2003
- Tibaldi S, D’Andrea F, Tosi E, Roeckner E (1997) Climatology of Northern Hemisphere blocking in the ECHAM model. *Clim Dyn* 13: 649–666
- Treidl RA, Birch EC, Sajecki P (1981) Blocking action in the Northern Hemisphere: a climatological study. *Atmosphere-Ocean* 19: 1–23
- Trigo IF, Davies TD, Bigg GR (1999) Objective climatology of cyclones in the Mediterranean region. *J Clim* 12: 1685–1696
- Trigo IF, Bigg GR, Davies TD (2002) Climatology of cyclogenesis mechanisms in the Mediterranean. *Mon Weather Rev* 130: 549–569
- Trigo RM, DaCamara CC (2000) Circulation weather types and their impact on the precipitation regime in Portugal. *Int J Climatol* 20: 1559–1581
- Trigo RM, Osborn TJ, Corte-Real JM (2002) The North Atlantic Oscillation influence on Europe: climate impacts and associated physical mechanisms. *Clim Res* 20: 9–17
- Tsou CH, Smith PJ (1990) The role of synoptic/planetary-scale interactions during the development of a blocking anticyclone. *Tellus* 42A: 174–193
- Tung KK, Lindzen RS (1979) A theory of stationary long waves. 1. A simple theory of blocking. 2. Resonant Rossby waves in the presence of realistic vertical shears. *Mon Weather Rev* 107: 735–750
- Verdecchia M, Visconti G, D’Andrea F, Tibaldi S (1996) A neural network approach for blocking recognition. *Geophys Res Lett* 23: 2081–2084
- Widmann M, Bretherton CS (2000) Validation of mesoscale precipitation in the NCEP reanalysis using a new gridcell dataset for the northwestern United States. *J Clim* 13: 1936–1950
- Wilby RL, O’Hare G, Barnsley N (1997) The North Atlantic Oscillation and the British Isles climate variability 1865–1995. *Weather* 52: 266–276
- White G (2000) Long-term trends in NCEP/NCAR Reanalysis. *Proc 2nd Int Conf on Reanalyse*, Reading, United Kingdom. World Meteorological Organization, Geneva Switzerland. WCRP-109 (WMO/TD985), 54–57
- Xie P, Arkin PA (1997) Global precipitation: a 17-year monthly analysis based on gauge observations, satellite estimates and numerical model outputs. *Bull Am Meteorol Soc* 78: 2539–2558
- Zolina O, Gulev SK (2002) Improving accuracy of mapping cyclone numbers and frequencies. *Mon Weather Rev* 129: 748–759